

RESEARCH ARTICLE | JUNE 25 2025

## Driven polymer translocation through a nanopore from a confining channel

Soheila Emamyari ; Jalal Sarabadani  ; Ralf Metzler ; Tapio Ala-Nissila 



*J. Chem. Phys.* 162, 244903 (2025)

<https://doi.org/10.1063/5.0269884>



### Articles You May Be Interested In

Theory of polymer translocation through a flickering nanopore under an alternating driving force

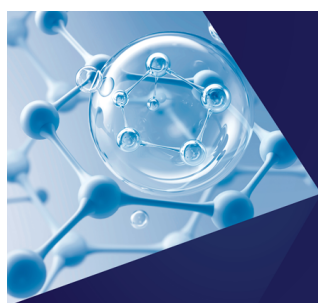
*J. Chem. Phys.* (August 2015)

Translocation of two-dimensional active polymers through nanopores using Langevin dynamics simulations

*J. Chem. Phys.* (May 2024)

Iso-flux tension propagation theory of driven polymer translocation: The role of initial configurations

*J. Chem. Phys.* (December 2014)



The Journal of Chemical Physics  
**Special Topics Open  
for Submissions**

[Learn More](#)

# Driven polymer translocation through a nanopore from a confining channel

Cite as: J. Chem. Phys. 162, 244903 (2025); doi: 10.1063/5.0269884

Submitted: 8 March 2025 • Accepted: 29 May 2025 •

Published Online: 25 June 2025



View Online



Export Citation



CrossMark

Soheila Emamyari,<sup>1</sup> Jalal Sarabadani,<sup>1,a)</sup> Ralf Metzler,<sup>2,3</sup> and Tapio Ala-Nissila<sup>4,5</sup>

## AFFILIATIONS

<sup>1</sup>School of Quantum Physics and Matter, Institute for Research in Fundamental Sciences (IPM), Tehran 19538-33511, Iran

<sup>2</sup>Institute of Physics and Astronomy, University of Potsdam, 14476 Potsdam, Germany

<sup>3</sup>Asia Pacific Centre for Theoretical Physics, Pohang 37673, Republic of Korea

<sup>4</sup>Department of Applied Physics and QTF Center of Excellence, Aalto University, P.O. Box 15600, FIN-00076, Aalto, Espoo, Finland

<sup>5</sup>Interdisciplinary Centre for Mathematical Modelling and Department of Mathematical Sciences, Loughborough University, Loughborough, Leicestershire LE11 3TU, United Kingdom

<sup>a)</sup> Author to whom correspondence should be addressed: [jalal@ipm.ir](mailto:jalal@ipm.ir)

## ABSTRACT

We consider the dynamics of pore-driven polymer translocation through a nanopore to a two-dimensional semi-infinite space when the chain is initially confined and equilibrated in a narrow channel. To this end, we use Langevin dynamics (LD) simulations and iso-flux tension propagation (IFTP) theory to characterize local and global dynamics of the translocating chain. The dynamics of the process can be described by the IFTP theory in very good agreement with the LD simulations for all values of confinement in the channel. The theory reveals that for channels with a size comparable to or less than the end-to-end distance of the unconfined chain, in which the blob theory works, the scaling form of the translocation time depends on both the chain contour length and the channel width. Conversely, for a very narrow channel, the translocation time only depends on the chain contour length and is similar to that of a rod due to the absence of spatial chain fluctuations.

Published under an exclusive license by AIP Publishing. <https://doi.org/10.1063/5.0269884>

## I. INTRODUCTION

Since the seminal experimental studies by Bezrukov *et al.*<sup>1</sup> and Kasianowicz *et al.*<sup>2</sup> and the theoretical work by Sung and Park,<sup>3</sup> a huge body of theoretical<sup>3–53</sup> and experimental<sup>54–64</sup> works has appeared to explain the underlying physical mechanisms during the process of polymer translocation (PT) through a nanopore. In addition to being of great theoretical interest as a dynamical nonequilibrium process, PT has a wide range of applications, such as RNA transport through nuclear membrane pores,<sup>65</sup> transfer of genes between bacteria,<sup>66</sup> using ratchets for filtration of polyelectrolytes,<sup>10</sup> and drug delivery and DNA sequencing.<sup>67–69</sup>

There are many variations of the PT process that have been studied to date. The translocation process can be either unbiased<sup>9,15,19,25</sup> or driven.<sup>6,16,26</sup> For the driven case, several different scenarios exist; for example, in the end-pulled case, an external driving force can be applied to the polymer head monomer<sup>41</sup> by an atomic force microscope (AFM)<sup>70</sup> or by magnetic or optical

tweezers.<sup>58,60,64,71,72</sup> The driving force can be localized inside the pore (pore-driven PT),<sup>16,26,35</sup> or it can be an effective force due to the interaction of the *trans*-side subchain with ambient active rods<sup>50</sup> or chaperones.<sup>12,13</sup> In the pore-driven case where the driving force acts on the monomers inside the nanopore, the driving force can be alternating and the nanopore can be flickering.<sup>27,38</sup> Both the pore-driven and end-pulled cases can be described by the iso-flux tension propagation (IFTP) theory.<sup>6,16,26,35</sup> In the unbiased or weakly driven PT, the entropic force resulting from fluctuations in the spatial configurations of the chain (entropy) plays an important role in the dynamics of the process, and a full theoretical understanding of PT in this limit is still missing.<sup>3</sup>

An interesting special case of PT is when there is a significant entropic force due to geometric confinement either on the *cis* or the *trans* side. In the latter case of polymer trapping, an external driving force is needed to overcome entropic repulsion due to confinement. In Refs. 28 and 51, the driven PT of a polymer from a semi-infinite *cis* side into a *trans* side channel was investigated. In the case where the

polymer is initially trapped, it can spontaneously escape the confinement or a confining potential well.<sup>20,73,74</sup> This process can be further facilitated by external driving. In Ref. 75, a pore-driven PT process was considered, where the polymer was confined in a channel on the *cis* side and then translocated to a semi-infinite compartment through a pore in the middle of the channel. Using Langevin Dynamics (LD) simulations and tension propagation arguments, the authors were able to characterize the dependence of PT on the channel diameter and obtain an analytic scaling form for the average translocation time  $\tau$ .

In this paper, we expand on the work in Ref. 75 by performing a detailed analysis of the local and global dynamics of the pore-driven PT process in two-dimensional (2D) space. We use the same setup according to which we drive a flexible self-avoiding polymer through a nanopore, and the polymer starts in a long confining channel on the *cis* side. It is forced through the nanopore by an external force that affects the monomers inside the pore (cf. Fig. 1). We characterize the dynamics of this process by performing a full analysis within the IFTP theory and derive the corresponding scaling forms for driven PT, including an analytic expression for  $\tau$  as a function of the chain length, driving force, confinement dimension, and effective channel friction. In addition, we present numerical results for the local chain dynamics using the waiting-time distribution, monomer number density, and other quantities, including monomer velocity distributions. These results significantly extend and generalize those in Ref. 75. Numerical data from the LD simulations are then compared with theory for the relevant physical quantities. The main focus here is the influence of the channel width  $D$  and the driving force  $f$  on the PT dynamics.

In the high-force limit in which the entropic force can be ignored, regardless of the width of the channel, the IFTP theory

predicts that  $\tau$  scales with the force as  $\tau \propto f^\beta$  with  $\beta = -1$ . However, the results of the LD simulations for a fixed large  $f$  show that  $|\beta| < 1$ , and it depends on  $D$ . It increases with increasing channel width due to the growth of fluctuations from  $-0.925 \pm 0.008$  to  $-0.900 \pm 0.003$ . For  $D > R_e$ , where  $R_e$  is the end-to-end distance of the unconfined chain, the force exponent settles to  $-0.900 \pm 0.003$  as the polymer is very weakly confined and fluctuations in the spatial polymer configurations do not increase. There are experimental results that have visualized the spatial conformations of DNA inside a confining micro- or nanochannel,<sup>76–80</sup> so we expect that comparing our results with the experimental observations will lead to a better understanding of this translocation process.

The structure of this paper is as follows: In Sec. II, the simulation model is explained in detail. Then, the IFTP theory is introduced in Sec. III. Results that include waiting time, translocation time, mean squared displacement, and monomer number density are presented in Sec. IV. Section V contains our summary and conclusions.

## II. SIMULATION MODEL

For the numerical LD simulations, we have used the LAMMPS software package.<sup>81</sup> The system under consideration is two-dimensional, composed of a linear, self-avoiding, fully flexible polymer initially on the *cis* side channel of width  $D$ , as depicted in Fig. 1(a). At the end of the channel, there is a membrane with a pore in the middle of the channel through which driven PT takes place. The membrane and channel walls are made up of fixed particles, each of size  $\sigma$ , that are located next to each other at a distance of  $\sigma$  (green beads in Fig. 1). The pore diameter is  $2\sigma$ , and the channel length is much larger than the polymer contour

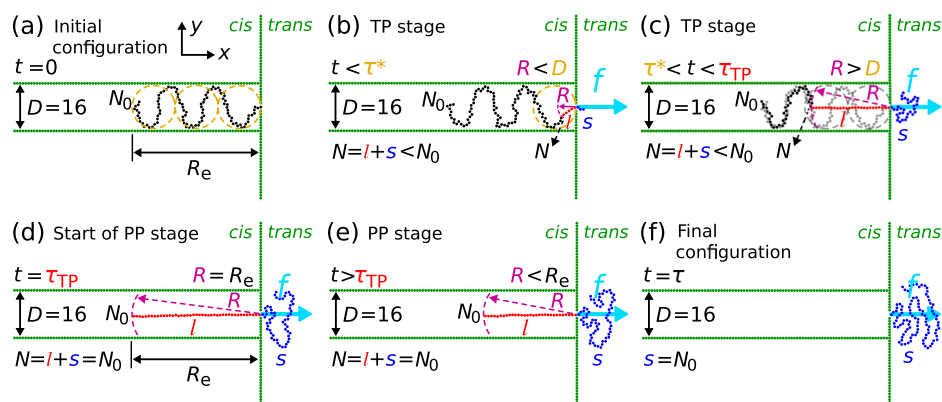


**FIG. 1.** (a) Polymer configuration inside the channel on the *cis* side just after equilibration at time  $t = 0$ . The contour length of the polymer is  $N_0 = 100$ , and  $D = 16$  is the channel width.  $R_e$  is the end-to-end distance of the polymer at  $t = 0$ , which is a function of  $D$  and  $N_0$ . The orange dashed circles show the blobs whose diameters are equal to the channel width here. The channel walls and the membrane are parallel to the  $x$  and  $y$  directions, respectively. The center of the pore is located in the middle of the channel at the origin  $(0, 0)$ . (b) Configuration of the polymer during the tension propagation (TP) stage when  $s$  monomers have already translocated to the *trans* side.  $f$  is the external driving force (denoted by the horizontal cyan vector) acting on the monomer(s) inside the pore in the positive  $x$  direction toward the *trans* side.  $R$  (denoted by the violet vector) is the location of the tension front at time  $t$ , and  $l$  is the number of red monomers under the tension so far, i.e.,  $N = l + s < N_0$ . Here,  $R$  is smaller than  $D$  for  $t < \tau^*$ , where  $\tau^*$  is the time at which  $R = D$ .  $N$  is the number of monomers that have been influenced by the tension so far, i.e.,  $N = l + s < N_0$ . (c) Polymer configuration during the TP stage when the tension front has not yet reached the last monomer of the polymer while  $R > D$ , i.e., for  $\tau^* < t < \tau_{TP}$ . Here, the chain in gray color shows the polymer configuration at  $t = 0$ , just to compare with the chain configuration at time  $t$ . Panel (d) is the same as (c), but the tension front has just reached the last monomer of the polymer at  $t = \tau_{TP}$  when  $R = R_e$ , and as all monomers are under tension,  $N = l + s = N_0$ . (e) The post-propagation stage of the translocation process at  $t > \tau_{TP}$ , where all monomers of the *cis* side are moving toward the pore. (f) The final configuration of the polymer just at the end of the translocation process at  $t = \tau$ , in which  $s = N_0$ .

length. The simulation box dimensions in the  $x$  and  $y$  directions are  $L_x = L_y = 210\sigma$ . The polymer is composed of  $N_0$  monomers [black beads in Fig. 1(a)] and is modeled by a bead-spring chain.<sup>82</sup> The consecutive bonded monomers interact with each other via a sum of Weeks–Chandler–Anderson (WCA)<sup>83</sup> and finitely extensible nonlinear elastic (FENE) potentials. The repulsive WCA potential is

$$U_{\text{WCA}}(r) = \begin{cases} U_{\text{LJ}}(r) - U_{\text{LJ}}(r_c) & \text{if } r \leq r_c, \\ 0 & \text{if } r > r_c, \end{cases} \quad (1)$$

where  $r$  is the monomer–monomer distance,  $r_c = 2^{1/6}\sigma$  is the cutoff radius, and  $U_{\text{LJ}}(r)$  is the Lennard-Jones (LJ) potential,

$$U_{\text{LJ}}(r) = 4\epsilon \left[ \left( \frac{\sigma}{r} \right)^{12} - \left( \frac{\sigma}{r} \right)^6 \right], \quad (2)$$

with  $\epsilon$  and  $\sigma$  as the depth of the potential and the monomer size, respectively. The FENE potential that connects the consecutive monomers is given by

$$U_{\text{FENE}}(r) = -\frac{1}{2}kR_0^2 \ln \left[ 1 - \left( \frac{r}{R_0} \right)^2 \right], \quad (3)$$

where  $k$  and  $R_0$  are the effective spring constant and the maximum extent of the bond between the neighboring monomers, respectively. All interactions between the non-bonded monomers of the polymer, monomers, and the membrane wall particles, and between monomers and the channel particles are governed by the repulsive WCA potential.

Using the LD simulation method, the equation of motion for the position vector of the  $i$ th monomer,  $\vec{r}_i$ , is given by

$$M\ddot{\vec{r}}_i = -\eta\dot{\vec{r}}_i - \vec{\nabla}U_i + \vec{\xi}_i(t), \quad (4)$$

where  $M$ ,  $\eta$ , and  $U_i$  are the monomer mass, the friction coefficient, and the sum of all interaction potentials experienced by the  $i$ th monomer, respectively.  $\vec{\xi}_i(t)$  is the thermal white noise vector at time  $t$  with zero mean  $\langle \vec{\xi}_i(t) \rangle = \vec{0}$  and correlation  $\langle \vec{\xi}_i(t) \cdot \vec{\xi}_j(t') \rangle = 4\eta k_B T \delta_{ij} \delta(t - t')$ .  $k_B$  and  $T$  are the Boltzmann constant and the temperature, respectively, and  $\delta_{ij}$  and  $\delta(t - t')$  are the Kronecker and Dirac delta functions, respectively.

$M$ ,  $\sigma$ , and  $\epsilon$  are chosen to be the units of mass, length, and energy, respectively.  $\sigma = 1$  is the diameter, and  $M = 1$  is the mass of each particle (monomers of the polymer or particles of the membrane and the channel walls). The values of the energy unit, solvent friction coefficient, and temperature are  $\epsilon = 1$ ,  $\eta = 0.7$ , and  $k_B T = 1.2$ , respectively. The simulation time step is  $dt = 0.001\tau_0$ , in which  $\tau_0 = \sqrt{M\sigma^2/\epsilon}$  is the simulation time unit. In addition, the maximum allowed distance between each two connected monomers is  $R_0 = 1.5$ , and  $k = 100$  (unless otherwise mentioned) is the spring constant in the FENE potential. The contour length of the polymer in LJ units is  $N_0 = 100$ .

The size of each bead in our model corresponds to the Kuhn length of a single-stranded DNA and is  $\sim 1.5$  nm, which is about the size of three nucleotides. As the mass of a nucleotide is about 312 amu, then the mass of each bead in our simulations is about 936 amu with the interaction strength of  $3.39 \times 10^{-21}$  J at room temperature ( $T = 295$  K). Consequently, the time and the force

units are obtained as 32.1 ps and 2.3 pN, respectively. Given the pore thickness  $1\sigma = 1.5$  nm (see Fig. 1) and the fact that the electric charge of each bead is equivalent to that of three single nucleotides (each with an effective charge of  $0.094e$ <sup>55,84</sup>), an external driving force of  $f = 4$  corresponds to a voltage of 306 mV across the pore.<sup>85</sup>

Before the PT process starts, one head bead of the polymer is fixed in the pore while the rest of the chain is carefully equilibrated within the channel over times much longer than the relaxation time of the end-to-end distance of the polymer. In addition, at this stage, a low value of the solvent friction  $\gamma = 0.1$  is used with a time step of  $dt = 0.005$ . After that, the integrator is run for the same time interval as with low friction, but for  $\gamma = 0.7$  with a time step of  $dt = 0.001$ . This procedure ensures that the chain has been fully equilibrated. After equilibration, the fixed head monomer is released, the pore driving force  $f$  is switched on, and the translocation process starts. It ends when the last tail bead has moved to the *trans* side, and the time taken defines the PT time  $\tau_i$  for each attempt  $i$ . To obtain sufficient statistics, data are averaged over 1000 independent PT events.

### III. THEORY

In Fig. 1(a), we show a typical equilibrium state of the system just before the translocation process ( $t = 0$ ) for a channel width  $D = 16$ . The end-to-end distance of the polymer at time  $t = 0$  is denoted by  $R_e$ , and it is a function of  $D$  and  $N_0$ . More details about the scaling form of  $R_e$  at  $t = 0$  can be found in Appendix A. Moreover, the orange dashed circles represent the blobs<sup>86</sup> whose diameters are equal to the channel width here.

As panel (b) in Fig. 1 shows, the external driving force  $f$  acts on the monomer(s) inside the pore. Here,  $s$  is the number of beads (in blue color) that have translocated to the *trans* side. The subchain on the *cis* side consists of two parts, a part with  $l$  monomers under tension (in red color) and an equilibrium part with the monomers that have not yet been affected by tension and have zero average velocity (in black color). The boundary between the two parts, denoted by  $N$ , defines the tension front position in the chain at a distance of  $R$  (violet arrow) from the nanopore. Figure 1(b) presents the system configuration for  $R < D$  at  $t < \tau^*$ , where  $t = \tau^*$  is the time at which  $R = D$ . As time passes with the propagation of tension along the backbone of the subchain on the *cis* side,  $R$  grows such that  $R > D$  for  $t > \tau^*$  [see Fig. 1(c)]. The stage where tension still propagates along the backbone of the polymer and has not reached the chain end on the *cis* side is called the tension propagation (TP) stage. Panels (b) and (c) in Fig. 1 present the TP stage of the translocation process. The TP time  $\tau_{\text{TP}}$  is the time at which the tension reaches the end of the polymer chain on the *cis* side. As shown in panel (d) of Fig. 1, tension has just reached the last monomer of the subchain on the *cis* side at time  $t = \tau_{\text{TP}}$ , and  $R = R_e$  applies. After that, in the post-propagation (PP) stage for  $t > \tau_{\text{TP}}$ , all monomers of the subchain on the *cis* side move toward the pore as shown in Fig. 1(e). Finally, panel (f) in Fig. 1 shows the final configuration of the system at the end of the translocation process at  $t = \tau$ , where  $\tau$  is the average translocation time and  $s = N_0$ .

To model the driven PT process explained above, we use the well-established IFTP theory.<sup>6,16,26,35</sup> We express all quantities in dimensionless units as identified by a tilde. They are denoted as  $\tilde{Z} \equiv Z/Z_u$ , where the units of length, time, velocity, monomer flux, friction, and force are indicated by the denominator, as  $s_u \equiv \sigma$ ,

$t_u \equiv \eta\sigma^2/(k_B T)$ ,  $v_u \equiv \sigma/t_u$ ,  $\phi_u \equiv k_B T/(\eta\sigma^2)$ ,  $\Gamma_u \equiv \eta$ , and  $f_u \equiv k_B T/\sigma$ , respectively. All parameters in LJ units do not have a tilde.

From the IFTP theory, the translocation process can be described by solving an equation of motion for the translocation coordinate  $\tilde{s}$ . To this end, one needs to know the tension force  $\tilde{\mathbb{F}}(\tilde{x}, \tilde{t})$  at distance  $\tilde{x}$  from the pore on the *cis* side. The force-balance equation for a differential element of the mobile part of the polymer chain on the *cis* side is  $d\tilde{\mathbb{F}}(\tilde{x}', \tilde{t}) = -\tilde{\phi}(\tilde{t})d\tilde{x}'$ . Here,  $\tilde{\phi}(\tilde{t}) = d\tilde{s}/d\tilde{t}$  is the monomer flux, and iso-flux means that the value of the monomer flux in the mobile domain is constant. Integrating the above force-balance equation from the pore located at  $\tilde{x}' = 0$  to the distance  $\tilde{x}' = \tilde{x}$ , the tension force at the distance  $\tilde{x}$  can be written as  $\tilde{\mathbb{F}}(\tilde{x}, \tilde{t}) = \tilde{\mathbb{F}}_0 - \tilde{x}\tilde{\phi}(\tilde{t})$ , in which  $\tilde{\mathbb{F}}_0 = \tilde{f} - \tilde{\eta}_p\tilde{\phi}(\tilde{t})$ , where  $\tilde{f}$  is the external driving force acting on the monomer(s) inside the nanopore and  $\tilde{\eta}_p$  is the pore friction. Using the fact that the tension force vanishes at the tension front, i.e.,  $\tilde{\mathbb{F}}(\tilde{x} = \tilde{R}, \tilde{t}) = 0$ ,  $\tilde{R}$  relates to the force at the entrance of the pore on the *cis* side as  $\tilde{\mathbb{F}}_0 = \tilde{R}(\tilde{t})\tilde{\phi}(\tilde{t})$ . Using the definition of the monomer flux in the above relation, the time evolution of the translocation coordinate  $\tilde{s}$  can be written as

$$[\tilde{\eta}_p + \tilde{R}(\tilde{t})] \frac{d\tilde{s}}{d\tilde{t}} = \tilde{f}, \quad (5)$$

where the effective friction inside the brackets is the sum of pore friction ( $\tilde{\eta}_p$ ) and friction due to the movement of the mobile part in the solvent  $\tilde{R}(\tilde{t})$ .

To solve Eq. (5), one needs to know the time evolution of  $\tilde{R}(\tilde{t})$ . By comparing the spatial configuration of the polymer chain at times zero and  $\tilde{t}$ , the equation of motion for  $\tilde{R}(\tilde{t})$  in the TP stage can be written as explained below. As shown in Fig. 1(c), the sum of the number of mobile monomers on the *cis* side  $\tilde{l}$  and the number of monomers on the *trans* side  $\tilde{s}$  is denoted by  $N$  ( $N = \tilde{l} + \tilde{s}$ ), which is less than the contour length of the polymer ( $N < N_0$ ) in the TP stage. Initially, at  $t = 0$ , there is no tension front yet, and thus at time  $\tilde{t}$  we can write  $\tilde{R}$  as the end-to-end distance of the polymer subchain with contour length  $N$  as schematically shown in Fig. 1(c).

If the channel is wide enough such that  $\tilde{D} > \tilde{R}(N_0) = \tilde{R}_e$  or we consider early stages of the translocation process during  $\tilde{t} < \tilde{\tau}^*$  [panel (b) in Fig. 1], where  $\tilde{D} > \tilde{R}(N)$ , then  $\tilde{R}$  is given by the standard Flory scaling form  $\tilde{R} = AN^\nu$ . Here,  $\nu = 3/4$  is the Flory exponent in two dimensions, and  $A$  is a constant of order unity. In the high-force limit when the mobile subchain on the *cis* side is fully straightened,  $\tilde{l}$  is replaced by the distance of the tension front location from the pore, i.e.,  $\tilde{l} = \tilde{R}$ , and using the definition of  $N$ , the following equation of motion for  $\tilde{R}$  must be solved:

$$\dot{\tilde{R}} = A(\tilde{R} + \tilde{s})^\nu. \quad (6)$$

In the opposite case of narrow channels, in which  $\tilde{D} < \tilde{R}(N_0)$ , during  $\tilde{\tau}^* < \tilde{t} < \tilde{\tau}_{TP}$  [panel (c) in Fig. 1]  $\tilde{R}$  depends on both  $\tilde{D}$  and  $N$ . For this case, employing the blob theory, one can write  $\tilde{R}$  as a function of  $\tilde{D}$  and  $N$ . In Fig. 1(a), the end-to-end distance of the polymer subchain inside each orange blob is written as  $\tilde{D} = Ag^\nu$ , where  $g$  is the number of monomers inside each blob. The number of blobs inside the channel is  $n_b = N_0/g$ . Then, at  $\tilde{t} = 0$ , the end-to-end distance of the chain inside the channel is given by  $\tilde{R}_e = n_b\tilde{D} = A^{1/\nu}N_0\tilde{D}^{1-1/\nu}$ , which is in agreement with the results of the LD simulations (for more details, see Appendix A). Performing the same procedure at time  $\tilde{t}$  in panel (c) in Fig. 1,  $\tilde{R}(\tilde{t})$  can be obtained as  $\tilde{R} = A^{1/\nu}N\tilde{D}^{1-1/\nu}$ ,

where  $N = \tilde{l} + \tilde{s}$  and in the high force limit, in which  $\tilde{l} = \tilde{R}$ , it can be cast to

$$\dot{\tilde{R}} = A^{1/\nu}(\tilde{R} + \tilde{s})\tilde{D}^{1-1/\nu}. \quad (7)$$

Thus, in the TP stage, the time evolution of  $\tilde{R}$  is given by solving either Eq. (6) or (7) in the relevant time regime.

In the PP stage, as the tail monomer (chain end) experiences the tension force, the whole *cis*-side subchain moves toward the pore. Performing a time derivative of the closure relation in the PP stage, which is  $N = \tilde{l} + \tilde{s} = N_0$ , in the high force limit ( $\tilde{l} = \tilde{R}$ ), the time evolution of  $\tilde{R}$  can be written as

$$\dot{\tilde{R}} = -\tilde{\phi}, \quad (8)$$

where  $\tilde{\phi} = d\tilde{s}/d\tilde{t}$  is the monomer flux. To describe the whole translocation process in the regime where the blob theory works, in the TP stage, Eqs. (5)–(7) must be solved, while in the PP stage, Eqs. (5) and (8) must be considered.

In the case of very narrow channels, in the TP stage, the monomers of the mobile part of the chain interact with the particles of the channel walls. However, in the PP stage, the *cis*-side mobile part moves like a rod and does not have significant interaction with the particles of the channel walls as long as  $D \gg r_c$ . Thus, the channel width should not influence the PP stage. However, in the TP stage, the chain-channel interactions induce an additional force  $-\tilde{\eta}_{ch}\tilde{\phi}(\tilde{t})d\tilde{x}'$  on a differential element of the mobile part of the polymer chain on the *cis* side, where  $\tilde{\eta}_{ch}$  is an effective friction from the walls. We have numerically evaluated  $\tilde{\eta}_{ch} \approx 0.2$  by fitting the waiting time from the IFTP theory to the LD simulation data. Thus, the effective force acting on  $d\tilde{x}'$  can be written as  $d\tilde{\mathbb{F}}(\tilde{x}', \tilde{t}) = -\tilde{\phi}(\tilde{t})d\tilde{x}' - \tilde{\eta}_{ch}\tilde{\phi}(\tilde{t})\Theta(\tilde{\tau}_{TP} - \tilde{t})d\tilde{x}'$ , where  $\Theta$  is the Heaviside step function. Then, the force balance equation for narrow channels is given by

$$\{\tilde{\eta}_p + \tilde{R}(\tilde{t})[1 + \tilde{\eta}_{ch}\Theta(\tilde{\tau}_{TP} - \tilde{t})]\} \frac{d\tilde{s}}{d\tilde{t}} = \tilde{f}. \quad (9)$$

To solve the above equation,  $\tilde{R}(\tilde{t})$  must be known. To find an equation for the time evolution of  $\tilde{R}$  for narrow channels, in which the blob theory breaks down, the initial configuration of the chain inside the narrow channel and its closure relation must be considered. The end-to-end distance of the polymer chain at  $\tilde{t} = 0$  is  $\tilde{R}_e = BN_0$ , where  $B \approx 0.77$ . Therefore, incorporating the mass conservation  $N = \tilde{l} + \tilde{s}$  in the TP stage in the high force limit, in which  $\tilde{l} = \tilde{R}$ , into  $\tilde{R} = BN$ , and performing its time derivative, the time evolution of  $\tilde{R}$  can be obtained as

$$\dot{\tilde{R}} = \frac{B\tilde{\phi}}{1 - B}. \quad (10)$$

In the PP stage, similar to the wider channels, the equation of motion for  $\tilde{R}$  is simply  $\dot{\tilde{R}} = -\tilde{\phi}$ . Therefore, to describe the translocation process for narrow channels in the TP stage, Eqs. (9) and (10) must be solved, while in the PP stage, Eq. (9) and  $\dot{\tilde{R}} = -\tilde{\phi}$  must be considered.

As mentioned above, the present study is devoted to investigating the IFTP theory of the translocation process in the high force limit. Similar systems can be investigated in the moderate (trumpet regime) and intermediate (stem-flower regime) force limits. For the trumpet and stem-flower regimes in the limit of  $D \gg R_e$ , where  $R_e$  is

the end-to-end distance of the polymer chain, driven translocation has been studied by employing the IFTP theory, and more details can be found in Ref. 35.

#### IV. RESULTS

In the present work, we have systematically studied the influence of the channel width and driving force on the pore-driven PT process in 2D. The values of the channel width are  $D = 2, 4, 8, 16, 24, 32, 40, 48, 56, 64, 72,$  and  $128$ . While the mean and the distribution of the translocation times are investigated for different values of the driving force  $f = 2, 4, 8, 16, 20, 40, 60, 80,$  and  $100$ , other results such as the waiting time (WT) distribution  $w$ , mean squared displacement (MSD) of monomers, monomer number density  $\rho$ , and the monomer velocity distributions are investigated in the high force (strong stretching) limit in which the driving force is fixed at  $f = 100$ .

##### A. Waiting time distribution

The distribution of waiting times  $w(s)$  as a function of the translocation coordinate  $s$  is an important quantity that reveals the translocation dynamics of a polymer at the monomer level and is defined as the average time that each monomer spends at the pore during the translocation process. The waiting time  $w(s)$  obtained from the LD simulations is shown in Fig. 2 as a function of the translocation coordinate  $s$  for a fixed value of the driving force  $f = 100$  and different values of the channel width  $D = 2 \dots 128$ . Results from the IFTP theory for  $D = 2 \dots 16$  and  $D > 32$  are in good agreement with the LD simulations. As expected, the pore friction varies with the channel width. The values of pore friction are  $\eta_p = 8, 8.5, 9, 9.5,$  and  $10$ , corresponding to the values of the channel width of  $D = 2, 4, 8, 16,$  and  $D > 32$ , respectively. Therefore, the IFTP theory presented in Sec. III can successfully explain the local dynamics of the translocation process at the monomer level. We note that both the influence of the drag force due to the crowding of the translocated monomers in the vicinity of the pore on the *trans* side and the spatial fluctuations of the chain configurations inside the channel are incorporated in the tension propagation theory through the effective pore friction coefficient  $\eta_p$ .

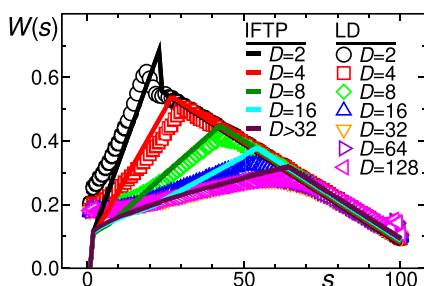


**FIG. 2.** Average waiting times  $w(s)$  extracted from the LD simulations for  $N_0 = 100$  as a function of the translocation coordinate  $s$ , for a fixed value of the driving force  $f = 100$  and different values of the channel width  $D = 2$  (black circles),  $4$  (red squares),  $8$  (green diamonds),  $16$  (blue triangles up),  $32$  (orange triangles down),  $64$  (violet triangles right), and  $128$  (magenta triangles left). The waiting times obtained numerically from the IFTP theory are denoted by the lines for  $D = 2$  (black line),  $4$  (red line),  $8$  (green line),  $16$  (cyan line), and  $D > 32$  (maroon line).

Figure 2 shows that for each  $D$ ,  $w(s)$  is nonmonotonic. It first increases and then decreases, which is typical for driven PT. In the TP stage ( $t < \tau_{TP}$ ), as time passes, more monomers join the mobile subchain on the *cis* side, and the friction experienced by the chain due to the solvent increases. Consequently, the dynamics slows down and  $w(s)$  grows. In the PP stage ( $t \geq \tau_{TP}$ ), when the whole *cis*-side subchain (influenced by the tension) moves toward the pore, the number of mobile monomers on the *cis* side and, therefore, the solvent friction decrease. Thus,  $w(s)$  decreases, too.

Moreover, Fig. 2 shows how confinement affects tension propagation. For the smallest value of  $D = 2 \ll R_c^\infty$ , where  $R_c^\infty \approx 30.3$  is the end-to-end distance for a polymer with  $N_0 = 100$  monomers in the semi-infinite free space, the chain fluctuations are strongly suppressed, and tension propagation terminates for the smallest value of  $s$  at which the WT maximizes. Increasing  $D$  increases the value of  $s$  for the maximum of  $w(s)$ , and finally for  $D \geq R_c^\infty$ , the location of the maximum value of  $w(s)$  is not affected by further increase in  $D$ .

##### B. Mean translocation time from LD simulations

The mean translocation time  $\tau$ , which identifies the global dynamics of the translocation process, is the average time that it takes for the whole polymer chain to traverse the pore and move to the *trans* side. Figure 3(a) shows the ensemble averaged  $\tau$  from LD simulations as a function of the driving force  $f$  for different values of the channel width  $D = 2 \dots 128$ . As expected,  $\tau$  decreases monotonically with increasing  $f$  for all values of  $D$ .

The inset in panel (a) shows the force exponent  $\beta$  from the scaling form  $\tau \propto f^\beta$  as a function of  $D$ . For the narrowest channel,  $D = 2$ , the force exponent is  $\beta = -0.925 \pm 0.008$ , and it increases

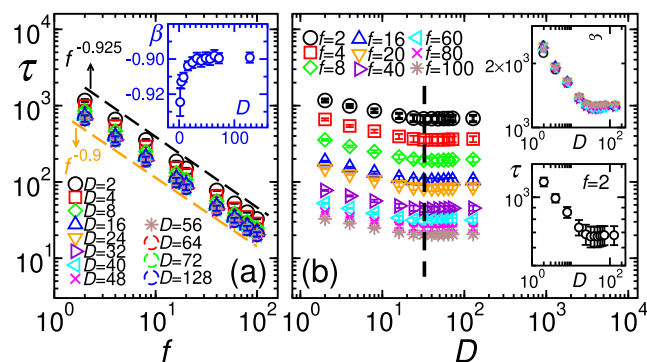


**FIG. 3.** (a) The average translocation time  $\tau$  from the LD simulations as a function of the driving force  $f$  for different values of the channel width  $D = 2$  (black circles),  $4$  (red squares),  $8$  (green diamonds),  $16$  (blue triangles up),  $24$  (orange triangles down),  $32$  (violet triangles right),  $40$  (cyan triangles left),  $48$  (magenta crosses),  $56$  (brown stars),  $64$  (red dashed circles),  $72$  (green dashed circles), and  $128$  (blue dashed circles). The inset shows the force exponent  $\beta$  (defined as  $\tau \propto f^\beta$ ) as a function of  $D$ . The numerically obtained average exponents fall between  $-0.925$  and  $-0.900$ , as indicated in the figure with dashed lines. (b) The average translocation time  $\tau$  as a function of the channel width  $D$  for different values of the driving force  $f = 2$  (black circles),  $4$  (red squares),  $8$  (green diamonds),  $16$  (blue triangles up),  $20$  (orange triangles down),  $40$  (violet triangles right),  $60$  (cyan triangles left),  $80$  (magenta crosses), and  $100$  (brown stars). The top inset shows the normalized average translocation time  $\tau/f^\beta$  as a function of  $D$  for all values of  $f$  as in the main panel. For the sake of better visibility, the bottom inset shows  $\tau$  as a function of  $D$  for a fixed value of  $f = 2$ . The error bars in the top inset in panel (b) are of the order of the symbol sizes or smaller.

with increasing  $D$  up to  $D \approx R_c^\infty$ . Then, for  $D > R_c^\infty$ ,  $\beta$  saturates to  $-0.900 \pm 0.003$ . The black and orange dashed lines in the main panel in Fig. 3(a) correspond to  $f^{-0.925}$  (for  $D = 2$ ) and  $f^{-0.900}$  (for  $D = 128$ ), respectively.

In Fig. 3(b), we plot  $\tau$  as a function of the channel width  $D$  for different values of the driving force  $f = 2 \dots 100$ . The top inset shows the normalized  $\tau/f^\beta$  as a function of  $D$  for all values of the driving force in the main panel. The data for  $f = 2$  are shown in the bottom inset for better visibility. The plot shows that for fixed  $f$ ,  $\tau$  decreases as  $D$  increases up to  $D \approx R_c^\infty$  (vertical black dashed-line in the main plot). This is due to the fact that for small  $D$ , the chain configuration is more extended along the channel axis and tension propagates faster, leading to increased drag from the *cis*-side sub-chain. For  $D > R_c^\infty$ ,  $\tau$  remains almost constant for fixed  $f$ . The top right inset in Fig. 3(b) shows data collapse for the normalized  $\tau/f^\beta$  as a function of  $D$ , where we have used the corresponding effective values of  $\beta(D)$ .

More details on the influence of driving force and channel width on the distribution of the translocation times are given in Appendix B.

### C. Analytic scaling form of translocation time

To analytically obtain the scaling form of the translocation time  $\bar{\tau}$  as a function of the chain contour length  $N_0$  and channel width  $\bar{D}$  from the IFTP theory, one needs to integrate  $N$  from zero to  $N_0$  in the TP stage and  $\bar{R}$  from  $\bar{R}(N_0)$  to zero in the PP stage. Tilde indicates the dimensionless units, as mentioned in Sec. III. For the cases when the blob theory works, combining the force balance Eq. (5) with the mass conservation laws  $N = \tilde{l} + \tilde{s}$  and  $N = \tilde{l} + \tilde{s} = N_0$  in the TP and PP stages, respectively, and then summing up the TP and PP times gives

$$\int_0^{\bar{\tau}} \tilde{f} d\tilde{t} = \int_{N=0}^{N=N_0} (\bar{R} + \tilde{\eta}_p) dN. \quad (11)$$

For the case  $\bar{D} < \bar{R}_c^\infty$ , the right hand side (RHS) of the above equation is split into different time regimes by comparing  $\bar{D}$  and  $\bar{R}$ , and the translocation time can be written as

$$\bar{\tau} = \frac{1}{\tilde{f}} \int_{N=0}^{N=N_*} \bar{R} dN + \frac{1}{\tilde{f}} \int_{N=N_*}^{N=N_0} \bar{R} dN + \tilde{\eta}_p N_0 / \tilde{f}, \quad (12)$$

where  $N_*$  is obtained as  $N_* = (\bar{D}/A)^{1/\nu}$  by using its definition  $\bar{R}(N_*) = AN_*^\nu = \bar{D}$ . In the first term in the RHS of Eq. (12), since  $\bar{R} < \bar{D}$ , the integral should be taken over  $\bar{R}(N) = AN^\nu$ , while in the second term  $\bar{R} > \bar{D}$  and the channel walls suppress polymer fluctuations, one must use  $\bar{R}(N) = A^{1/\nu} \bar{D}^{1-1/\nu} N$ . Using the definitions of  $N_*$  and the proper closure relation for  $\bar{R}$  in Eq. (12), the scaling form of the translocation time is obtained as

$$\bar{\tau} = \frac{\bar{D}^{1+\nu}}{\tilde{f} A^{1/\nu}} \left( \frac{1}{1+\nu} - \frac{1}{2} \right) + \frac{N_0^2}{2\tilde{f}} A^{1/\nu} \bar{D}^{1-1/\nu} + \tilde{\eta}_p \frac{N_0}{\tilde{f}}. \quad (13)$$

According to this result, for the present case where  $\nu = 3/4$ ,  $\tau$  decreases with increasing  $D$ , which is in agreement with our LD data in Fig. 3(b). A similar equation with the same  $N_0$ -dependence has already been derived in Ref. 75.

For channels with  $\bar{D} > \bar{R}_c^\infty$ , Eq. (11) does not need to be split. Using  $\bar{R}(N) = AN^\nu$ , the scaling form of the translocation time becomes

$$\bar{\tau} = \frac{1}{\tilde{f}} \frac{A}{1+\nu} N_0^{1+\nu} + \tilde{\eta}_p \frac{N_0}{\tilde{f}}, \quad (14)$$

which is identical to that of unconfined pore-driven translocation.<sup>35</sup>

For a very narrow channel ( $D = 2$ ), the blob theory does not work, as mentioned in Sec. III. The result of the IFTP theory (WT), which is confirmed by the results of the LD simulations, is shown for  $D = 2$  in Fig. 2 (black line and black circles in Fig. 2). In this case, in the TP stage, the mobile monomers on the *cis* side experience a dynamical frictional force due to the channel walls, as mentioned in Sec. III to obtain Eq. (9). On the other hand, in the PP stage, the chain is almost unaffected by the channel walls, as all mobile monomers of the chain on the *cis* side move together like a rod toward the pore. Therefore, combining the force balance equation  $[\tilde{\eta}_p + (1 + \tilde{\eta}_{ch})\bar{R}](d\tilde{s}/d\tilde{t}) = \tilde{f}$  with mass conservation  $N = \tilde{l} + \tilde{s}$  in the TP stage, and equation  $(\tilde{\eta}_p + \bar{R}) \frac{d\tilde{s}}{d\tilde{t}} = \tilde{f}$  with  $N = \tilde{l} + \tilde{s} = N_0$  in the PP stage, and summing up the TP and PP times yields

$$\int_0^{\bar{\tau}} \tilde{f} d\tilde{t} = \int_{N=0}^{N=N_0} [(1 + \tilde{\eta}_{ch})\bar{R} + \tilde{\eta}_p] dN - \int_{\bar{R}=0}^{\bar{R}=\bar{R}(N_0)} \tilde{\eta}_{ch} \bar{R} d\bar{R}. \quad (15)$$

Here, the effective channel friction  $\eta_{ch} = 0.2$ , and  $\bar{R}(N) = BN$  with  $B \approx 0.77$  is the closure relation for the end-to-end distance of a mobile subchain with  $N$  monomers inside a narrow channel. Using the above closure relation inside Eq. (15), the scaling form of the translocation time is written as

$$\bar{\tau} = \frac{1}{\tilde{f}} \left[ \frac{(1 + \tilde{\eta}_{ch})B}{2} - \frac{\tilde{\eta}_{ch}B^2}{2} \right] N_0^2 + \frac{1}{\tilde{f}} \tilde{\eta}_p N_0, \quad (16)$$

where the prefactor  $(1 + \tilde{\eta}_{ch})B/2 - \tilde{\eta}_{ch}B^2/2 \approx 0.4$  for the present model.

### D. Mean squared displacement

Next, we study PT by investigating the dynamics of the chain in more detail. To this end, we consider the time-dependence of the mean squared fluctuation of the position  $x(t)$  defined by

$$\text{MSD} = \langle [x(t) - x(0)]^2 \rangle. \quad (17)$$

This quantity is computed for the end monomer (tail) of the chain, the center of mass (CM) of the chain, and the CM of the *cis*-side subchain (CM<sub>c</sub>). In addition, we have computed the time-averaged MSD, MSD<sub>t-ave</sub>, defined as

$$\text{MSD}_{t\text{-ave}}(j\Delta T) = \frac{1}{n-j} \sum_{i=0}^{n-1-j} \{x[(i+j)\Delta t] - x(i\Delta t)\}^2, \quad (18)$$

where  $j = 1, 2, 3, \dots, n-1$ . In this equation, the  $x$  component of the position is saved at times with time lags  $\Delta t$  as  $x(0)$ ,  $x(\Delta t)$ ,  $x(2\Delta t)$ ,  $\dots$ ,  $x[(n-1)\Delta t]$ . For a non-ergodic system, MSD<sub>t-ave</sub> will be different from the ensemble-averaged MSD.<sup>87-91</sup> In an ergodic process, the ensemble and the long-time averages are similar.

Figures 4(a)–4(c) present ensemble averages of the horizontal position  $\langle x \rangle$  of the tail (end monomer) (black line), the CM of the

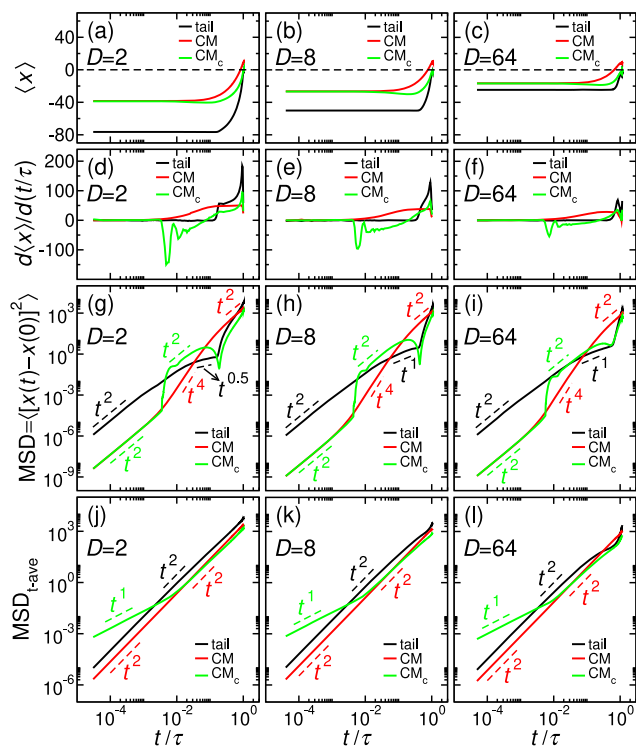


**FIG. 4.** (a) The ensemble average of the horizontal position ( $x$ ) of the tail (black line), center of mass of the whole chain (CM) (red line), and center of mass of the subchain in the *cis* side ( $CM_c$ ) (green line) as a function of the normalized time  $t/\tau$  for fixed values of the driving force  $f = 100$  and the channel width  $D = 2$ . Panels (b) and (c) are the same as (a), but for  $D = 8$  and  $64$ , respectively. Panels (d)–(f) are the ensemble averages of the slopes  $d\langle x \rangle/d(t/\tau)$  corresponding to the curves in panels (a)–(c). (g) Ensemble-averaged MSD as a function of normalized time  $t/\tau$  for the tail (black line), CM (red line), and  $CM_c$  (green line) for  $f = 100$  and  $D = 2$ . Panels (h) and (i) are the same as (g), but for  $D = 8$  and  $64$ , respectively. (j) Time-averaged MSD,  $MSD_{t-ave}$ , as a function of  $t/\tau$  for the tail (black line), CM (red line), and  $CM_c$  (green line) for  $f = 100$  and  $D = 2$ . Panels (k) and (l) are the same as panel (j) but for  $D = 8$  and  $64$ , respectively. All slopes of the dashed lines in (g)–(i) and (j)–(l) are guides to the eye.

whole chain (red line), and the CM of the *cis*-side subchain  $CM_c$  (green line) as a function of the normalized time  $t/\tau$  for fixed values of the driving force  $f = 100$  and for different channel widths  $D = 2, 8$ , and  $64$ . The value of  $\langle x \rangle$  starts to increase when the tension reaches the tail monomer, which, for smaller  $D$ , happens at smaller values of the normalized time. For all values of  $D$ ,  $\langle x \rangle$  of CM (red line) increases as the monomers of the chain are translocated to the *trans* side and eventually becomes positive as the number of translocated monomers on the *trans* side becomes sufficiently large. Moreover, the green lines in panels (a)–(c) correspond to the position of the *cis*-side subchain CM,  $CM_c$ . They show that  $CM_c$  first moves away from the pore (as the number of monomers in the mobile domain decreases compared to the number of monomers in the same spatial domain in the equilibrium state at  $t = 0$ ), and then it approaches the pore. Finally, at the end of the translocation process at  $t/\tau = 1$ , the value of  $\langle x \rangle$  for  $CM_c$  becomes zero.

Panels (d)–(f) present the slopes  $d\langle x \rangle/d(t/\tau)$  corresponding to the curves in panels (a)–(c). As can be seen, the slope for the

position of the tail monomer (in black color) starts to increase when the tension reaches the tail monomer, which for smaller  $D$  happens at smaller values of the normalized time. The slope for the position of  $CM_c$  (in green color) at short times is zero and then becomes negative as the location of  $CM_c$  moves toward the pore. As time passes and the  $CM_c$  approaches the pore, the slopes become positive. The slope for the position of CM (in red color) is zero at early times and positive at the intermediate and long time regions.

In Fig. 4(g), the ensemble-averaged MSD is shown as a function of  $t/\tau$  for the tail (black line), CM (red line), and  $CM_c$  (green line) for  $f = 100$  and  $D = 2$ . Panels (h) and (i) are the same as panel (g) but for  $D = 8$  and  $64$ , respectively. In all time regimes, the behavior of MSDs for the tail (and also for the CM) is similar for different values of  $D$ . The MSDs for the tail monomer [black lines in panels (g)–(i)] scale as  $t^2$  at early times and then show more complicated behavior when the PP stage starts. In contrast, MSDs for CM [red lines in panels (g)–(i)] show smoother behavior, scaling initially also as  $t^2$ . In addition, the MSDs for  $CM_c$  [green lines in panels (g)–(i)] scale again as  $t^2$  at early times but then follow the black curves at late times. The sharp valleys in the green curves represent the transition from TP to PP.

In Fig. 4(j),  $MSD_{t-ave}$  (averaged over 75 independent trajectories) is shown as a function of the normalized time  $t/\tau$  for the tail (black line), CM (red line), and  $CM_c$  (green line) for fixed values of the driving force  $f = 100$  and the channel width  $D = 2$ . Panels (k) and (l) are the same as panel (j) but for  $D = 8$  and  $64$ , respectively. As panels (j)–(l) clearly show,  $MSD_{t-ave}$  for the tail and CM scales as  $t^2$  for almost the entire translocation process for all values of  $D$ . On the other hand, the slope of  $MSD_{t-ave}$  of the  $CM_c$  (green line) crosses over from linear dependence to  $t^2$ . At very late times for  $D = 8$  and  $64$ , there is a slight bend in the tail curve indicating a transition from TP to PP.

## E. Monomer density

Finally, we study the time evolution of the monomer number density  $\rho(x, y)$  (the number of monomers per unit area), where the average spatial configuration of the polymer is investigated as a function of time during the translocation process. To calculate  $\rho$ , the 2D simulation box is divided into square unit cells of size  $1 \times 1$  each. The number of monomers in each unit cell is counted at a given moment for each trajectory and divided by the contour length of the polymer. In the end, the averaging is done over 1000 independent trajectories. Figure 5(a) shows the monomer number density at different normalized times  $t/\tau = 0 \dots 1.0$  for fixed values of the driving force  $f = 100$  and channel width  $D = 2$ . Panels (b) and (c) are the same as panel (a), but for different values of  $D = 8$  and  $64$ , respectively. For the sake of better visibility, the monomer number density of the *cis* side (inside the channel) is magnified and separately shown below the actual channel in panels (a) and (b).

As shown in panel (a) of Fig. 5, in this case, the polymer translocates in a rodlike manner in the channel, forming a coil at the *trans* side. Figure 5(b) shows that increasing the channel width to  $D = 8$  causes the chain to extend in the  $y$  direction until the tension front reaches the end. Finally, panel (c) shows that for  $D = 64$ , there is no contact between the chain and the particles on the channel walls since  $D > R_c^\infty$ .

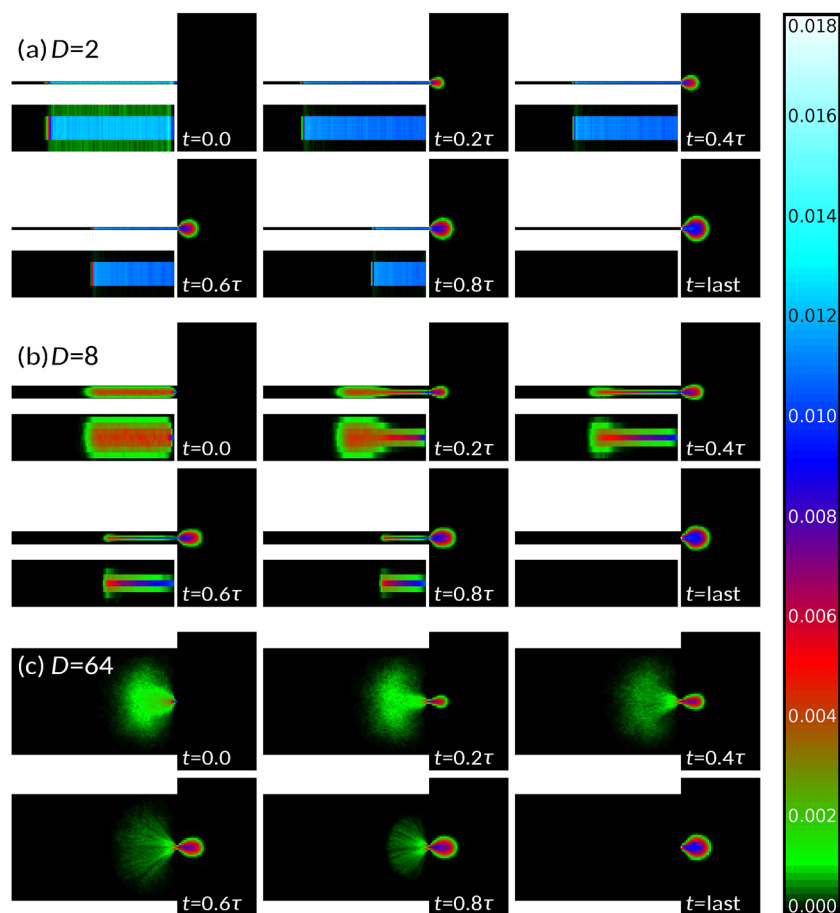


**FIG. 5.** (a) Monomer number density  $\rho(x, y)$  for fixed values of the driving force  $f = 100$  and the channel width  $D = 2$  at different times  $t/\tau = 0, 0.2, 0.4, 0.6, 0.8$ , and at the last snapshot. Panels (b) and (c) are the same as panel (a), but for other values of the channel width,  $D = 8$  and  $64$ , respectively. For the sake of better visibility,  $\rho(x, y)$  of the *cis* side (channel) is magnified and shown below each actual channel in panels (a) and (b).

## V. SUMMARY AND CONCLUSIONS

In this work, we have revisited the problem of pore-driven PT from a confining channel into semi-infinite free space. To this end, we have employed the IFTP theory to analytically calculate the scaling form for the average translocation time as a function of chain length, driving force, confinement, and channel friction. The IFTP theory can quantitatively explain the local waiting times as well as global dynamics, as given by the translocation time for the PT process for different values of channel width. The theory includes all cases from a highly confining channel where the blob theory breaks down, to intermediate channel widths where the blob theory applies, and finally to wide channels where spatial confinement becomes irrelevant.

First, for highly confining channels with  $D \ll R_e^\infty$  comparison between the waiting time from LD simulations and from the IFTP theory reveals that in the TP stage, interactions between the mobile monomers with the channel walls induce dynamic friction that is proportional to the size of the mobile domain at the *cis* side. In the PP stage, the mobile monomers move in a rodlike fashion inside the channel and significantly interact with the channel walls. Consequently, IFTP theory shows that the translocation time is similar to that of a rod and scales as  $\bar{\tau} \propto N_0^2$ .<sup>43</sup>

Second, for a channel of an intermediate width  $1 \ll D < R_e^\infty$ , we have used the blob theory in conjunction with the IFTP theory. The predictions on local and global PT dynamics are again in full agreement with the LD simulations. The scaling form of the translocation time depends on both the chain contour length and the channel diameter and agrees with those in Ref. 75 in the appropriate limits.

Third, for wide channels with  $D > R_e^\infty$ , both the IFTP theory and LD simulations recover the well-known results for a system with a semi-infinite space on the *cis* side, where the IFTP theory shows that the translocation time scales as  $\bar{\tau} \propto N_0^{1+\nu}$ .<sup>35</sup>

Finally, we have further characterized the details of the local and global chain dynamics by investigating the distribution of translocation times (cf. Appendix B) and the dependence of the MSDs of the tail, CM, and CM of the *cis*-side subchain, the time evolution of the monomer number density, and monomer velocity (cf. Appendix C) on the channel width at constant driving force in the high force limit. Our detailed analysis of the global and local chain dynamics as a function of the relevant parameters thus gives a complete picture of the PT dynamics from confined channels to free space and can be used to interpret and analyze related experiments of PT dynamics and biopolymer sequencing with nanopores.

Although the IFTP theory is valid for the 3D case as well, there are additional effects that need to be considered. For long chains, it

would be interesting to study the effect of knotting and unknotting dynamics of the polymer chain inside the channel on the dynamics of the polymer translocation through a nanopore and to develop the corresponding IFTP theory.<sup>92,93</sup>

## ACKNOWLEDGMENTS

S.E. and J.S. acknowledge the Iran National Science Foundation: “This work is based upon research funded by the Iran National Science Foundation (INSF) under Project No. 4026895.” R.M. acknowledges the German Science Foundation (DFG, Grant Nos. ME 1535/16-1 and ME 1535/13-1) for the support. T.A.-N. has been supported in part by the Academy of Finland Grant No. 353298 under the European Union—NextGenerationEU instrument. R.M. acknowledges funding from NSF-BMBF CRCNS through Grant No. 2112862/STAXS.

## AUTHOR DECLARATIONS

### Conflict of Interest

The authors have no conflicts to disclose.

## Author Contributions

**Soheila Emamyari:** Conceptualization (equal); Formal analysis (lead); Visualization (equal); Writing – review & editing (equal). **Jalal Sarabadani:** Conceptualization (equal); Writing – original draft (lead); Writing – review & editing (equal). **Ralf Metzler:** Conceptualization (equal); Writing – review & editing (equal). **Tapio Ala-Nissila:** Conceptualization (equal); Writing – review & editing (equal).

## DATA AVAILABILITY

The data in the figures are available at <https://doi.org/10.5281/zenodo.15394248>.

## APPENDIX A: POLYMER SCALING FROM BLOB THEORY IN A CHANNEL

To study the scaling of the polymer chain in a channel, we consider the radius of gyration (RG)  $R_g$  and end-to-end distance  $R_e$ . The ensemble averages  $\langle \dots \rangle$  of  $R_g$  and  $R_e$  for a polymer chain with a contour length of  $N$  are given by<sup>96</sup>  $R_g^2 = \frac{1}{N} \sum_{i=1}^N \langle (\vec{R}_i - \vec{R}_{CM})^2 \rangle$  and  $R_e^2 = \langle (\vec{R}_N - \vec{R}_1)^2 \rangle$ , respectively, where  $\vec{R}_i$  and  $\vec{R}_{CM}$  are the position vectors of the  $i$ th monomer and the center of mass of the chain, respectively.

As mentioned in Sec. III, using the blob theory, the end-to-end distance of a chain confined in a channel with a diameter of  $D$  is given by  $R_e = NA^{1/\nu} D^{1-1/\nu}$ . Figure 6(a) compares the results of LD simulations with those of the blob theory for  $R_g$  and  $R_e$ . In panel (a) of Fig. 6,  $R_g^2$  (orange circles) and  $R_e^2$  (cyan squares) of the initial configuration of the polymer inside the channel at  $t = 0$  are plotted as a function of the channel width  $D$ . As can be seen, as  $D$  increases, the values of both  $R_g^2$  and  $R_e^2$  decrease, and in the regime in which  $D > R_e (D = 128) \approx 30.32$ , they remain almost constant. The blue and red fitted dashed lines represent  $(100 \times D^{1-\nu})^2$  and  $(29 \times D^{1-\nu})^2$  with  $\nu = 3/4$ , respectively. Therefore, we conclude that the results of LD simulations are in very good agreement with the blob theory.

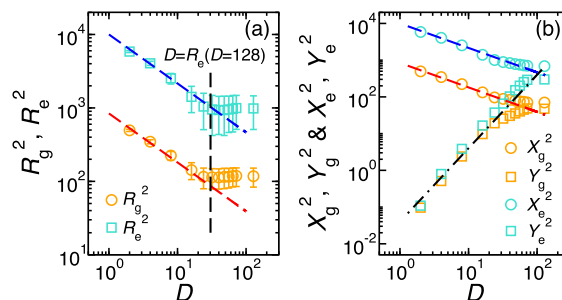


**FIG. 6.** (a) The average squared gyration radius  $R_g^2$  (orange circles) and the average squared end-to-end distance  $R_e^2$  (cyan squares) of the initial configuration of the chain at  $t = 0$  inside the channel as a function of the channel width  $D$ . The blue and the red dashed lines represent  $(100 \times D^{1-\nu})^2$  and  $(29 \times D^{1-\nu})^2$  with  $\nu = 3/4$ , respectively. The black vertical dashed line is  $D = 30.32$ . (b) The average squared radius of gyration in the  $x$  and  $y$  directions,  $X_g^2$  (orange circles) and  $Y_g^2$  (orange squares), and the average squared end-to-end distance in the  $x$  and  $y$  directions,  $X_e^2$  (cyan circles), and  $Y_e^2$  (cyan squares) of the initial configuration at  $t = 0$ , respectively, as a function of the channel width  $D$ . The blue and the red dashed lines are the same as of panel (a). The black dashed-dotted line is  $(0.2 \times D)^2$ .

Panel (b) in Fig. 6 shows the average of the square of the RG and the end-to-end distance in the  $x$  and  $y$  directions as  $X_g^2$  (orange circles) and  $Y_g^2$  (orange squares), and as  $X_e^2$  (cyan circles) and  $Y_e^2$  (cyan squares), respectively, for the initial ( $t = 0$ ) configuration of the chain inside the channel as a function of  $D$ . The blue and red dashed lines are the same as those in panel (a). The black dashed-dotted line is  $(0.2 \times D)^2$  and is obtained by fitting to the data in the regime of  $D < R_e (D = 128)$ .

It should be mentioned that in the present study, we investigate the translocation of a self-avoiding flexible chain through a nanopore, where both the persistence length and the chain width are of the order of unity. Therefore, we have employed the blob model (the De Gennes regime) to obtain the scaling form of the chain conformation inside the channel. However, for a semiflexible polymer translocation through a nanopore starting from a confining channel, several length scales are involved, e.g., channel width, polymer persistence length, its width, and polymer contour length, which must be compared to each other to identify if the blob theory is valid. Indeed, for the latter case, one can use the results of Refs. 94 and 95, where the existence of two transition regimes between weak (the De Gennes regime) and strong (the Odijk regime) confinements has been demonstrated.

## APPENDIX B: DISTRIBUTION OF TRANSLOCATION TIMES

In this appendix, we present LD results for the probability density function of translocation times  $P(\tau_i)$ . In Fig. 7(a),  $P(\tau_i)$  is shown as a function of individual translocation times  $\tau_i$  for a fixed value of the channel width  $D = 2$  and different values of the driving force  $f = 2 \dots 100$ . Panels (b) and (c) are the same as panel (a) but for other values of the channel width,  $D = 8$  and  $64$ , respectively. For fixed  $D$ , increasing  $f$  obviously decreases the average  $\tau$ , and  $P(\tau_i)$  becomes narrower. In fact, as  $f$  decreases, the spatial fluctuations of

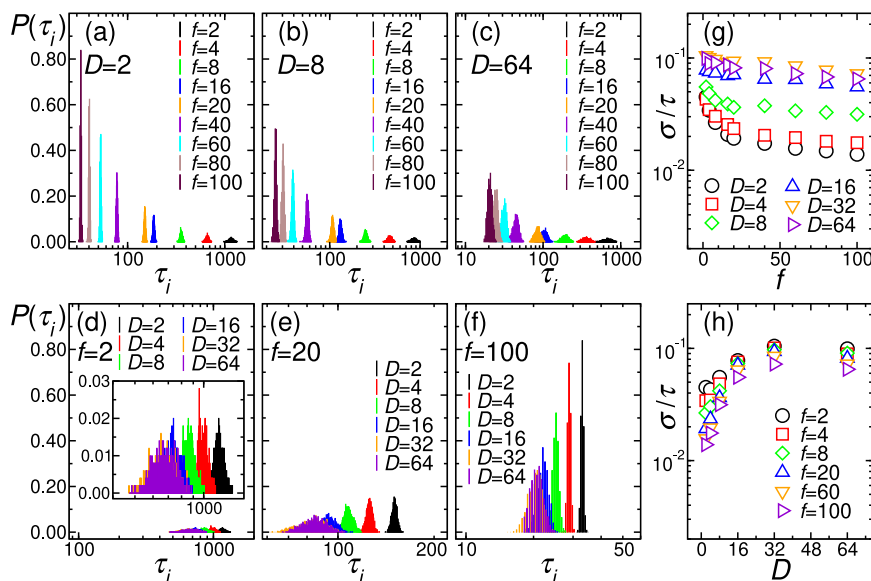


**FIG. 7.** (a) Probability density function of the translocation times  $P(\tau_i)$  as a function of the translocation time  $\tau_i$  for a fixed value of the channel width  $D = 2$  and different values of the driving force  $f = 2$  (black bars), 4 (red bars), 8 (green bars), 16 (blue bars), 20 (orange bars), 40 (violet bars), 60 (cyan bars), 80 (brown bars), and 100 (maroon bars). Panels (b) and (c) are the same as panel (a) but for other values of the channel width,  $D = 8$  and 64, respectively. (d)  $P(\tau_i)$  as a function of  $\tau_i$ , for a fixed value of the driving force  $f = 2$  and different values of the channel width  $D = 2$  (black bars), 4 (red bars), 8 (green bars), 16 (blue bars), 32 (orange bars), and 64 (violet bars). Panels (e) and (f) are the same as panel (d) but for different values of the driving force,  $f = 20$  and 100, respectively. The inset in panel (d) corresponds to the magnified main panel for better visibility. (g) Normalized value of the standard deviation  $\sigma/\tau$  as a function of  $f$  for different values of the channel width  $D = 2$  (black circles), 4 (red squares), 8 (green diamonds), 16 (blue triangles up), 32 (orange triangles down), and 64 (violet triangles right). (h)  $\sigma/\tau$  as a function of  $D$  for different values of the driving force  $f = 2$  (black circles), 4 (red squares), 8 (green diamonds), 20 (blue triangles up), 60 (orange triangles down), and 100 (violet triangles right).

the configurations of the *cis*-side subchain increase significantly, so the fluctuations of the translocation times also increase.

In Fig. 7(d),  $P(\tau_i)$  is shown as a function of translocation time  $\tau_i$  for a fixed value of the driving force  $f = 2$  and different values of the channel width  $D = 2 \dots 64$ . Panels (e) and (f) are the same as panel (d) but for other values of the driving force,  $f = 20$  and 100, respectively. For better visibility, the inset in panel (d) shows the magnified main panel. As can be seen for smaller values of  $D$ , increasing the value of  $f$  leads to an increase in the separation of  $P(\tau_i)$ 's, while this is not the case for larger values of  $D$ , in which, for different values of  $f$ , the probability density functions show an overlap.

In Fig. 7(g), the normalized standard deviation of translocation times  $\sigma/\tau$  is shown as a function of  $f$  for different values of the channel width  $D = 2 \dots 64$ . It is clear that  $\sigma/\tau$  decreases monotonically as  $f$  increases for all values of  $D$ , and the reduction of  $\sigma/\tau$  with respect to  $f$  is more pronounced for smaller values of  $D$ .

Moreover,  $\sigma/\tau$  is displayed in panel (h) as a function of  $D$  for different values of the driving force  $f = 2 \dots 100$ . As can be seen, for each value of  $f$ ,  $\sigma/\tau$  increases as  $D$  increases. At constant  $D$ , the deviation of  $\sigma/\tau$  with respect to  $f$  is more pronounced for larger values of  $D$  than for smaller ones.

### APPENDIX C: MONOMER VELOCITIES FOR THE TRANSLOCATION COORDINATE

Here, the dynamics of the *cis*-side subchain and the tension front are investigated by studying the velocity distribution of each

individual monomer at different moments during the translocation process. In Fig. 8(a), the  $x$  component of the monomer velocity  $v_x$  is plotted as a function of the translocation coordinate  $s$  for fixed values of  $D = 2$  and  $f = 100$  at different times  $t/\tau = 0.05 \dots 0.80$ . Panels (b) and (c) are the same as panel (a), but for other values of the channel width,  $D = 8$  and 64, respectively. In each curve, the left side of the open circle corresponds to the velocity of the translocated monomers to the *trans* side, and its right side shows the velocity of the monomers on the *cis* side at the corresponding time.

After equilibration at  $t = 0$ , all monomers have zero mean velocity, as monomers have not experienced any tension yet. As shown in Fig. 8, for each value of  $D$ , the number of monomers with non-zero velocity increases as time passes, i.e., more monomers join the mobile part of the chain on the *cis* side. Moreover, for smaller values of  $D$ , the last monomer feels the tension (joins to the mobile part) at smaller values of  $t/\tau$ . Therefore, for smaller values of  $D$ , the PP stage has a more significant contribution to the mean translocation time than the TP stage. Conversely, in the case where the channel width has larger values, i.e.,  $D > R_c^\infty$ , it takes longer for the tension to reach the last monomer, and therefore the TP stage has a larger contribution to the mean translocation time than the PP stage. In addition, panels (a)–(c) show that in the TP stage ( $t < \tau_{TP}$ ) the velocity of the mobile part of the chain on the *cis* side decreases with time, originating from the fact that as time passes more monomers join the mobile part and the effective friction increases, slowing down the dynamics. Conversely, in the PP stage ( $t > \tau_{TP}$ ), the velocity of the mobile monomers on the *cis* side increases with time due to the reduction in friction.

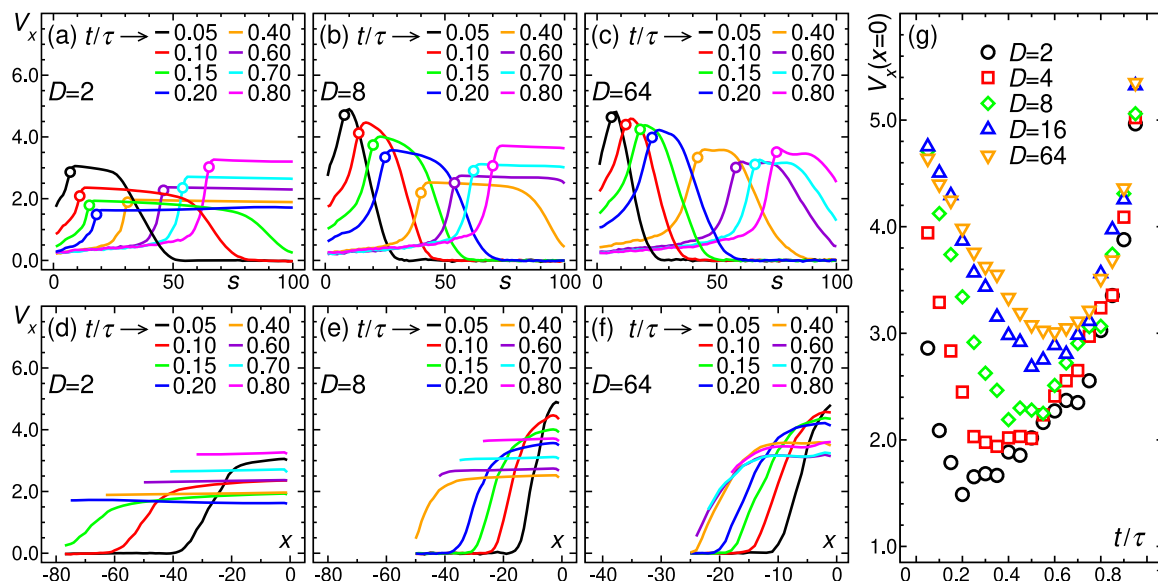


**FIG. 8.** (a) The  $x$  component of the monomer average velocity  $v_x$  as a function of the translocation coordinate  $s$  for fixed values of  $D = 2$  and  $f = 100$  at different times  $t/\tau = 0.05$  (black line), 0.10 (red line), 0.15 (green line), 0.20 (blue line), 0.40 (orange line), 0.60 (violet line), 0.70 (cyan line), and 0.80 (magenta line). Panels (b) and (c) are the same as panel (a), but for other values of the channel width,  $D = 8$  and 64, respectively. The open circle on each curve shows the mean value of the index of the monomer inside the pore at the corresponding time. (d) The  $x$  component of the monomer average velocity  $v_x$  as a function of  $x$  in the *cis* side, for fixed values of  $D = 2$  and  $f = 100$  at different times  $t/\tau = 0.05$  (black line), 0.10 (red line), 0.15 (green line), 0.20 (blue line), 0.40 (orange line), 0.60 (violet line), 0.70 (cyan line), and 0.80 (magenta line). Here,  $x = 0$  is the location of the pore. Panels (e) and (f) are the same as panel (d), but for other values of the channel width,  $D = 8$  and 64, respectively. Here,  $|x|$  is the distance from the pore on the *cis* side. (g) The average velocity of monomer(s) inside the pore  $v_x(x = 0)$  as a function of  $t/\tau$  for a fixed value of driving force  $f = 100$  and different values of the channel width  $D = 2$  (black circles), 4 (red squares), 8 (green diamonds), 16 (blue triangles up), and 64 (orange triangles down).

Furthermore, in Fig. 8(d), the mean value of the  $x$  component of the monomer velocity  $v_x$  is shown as a function of the  $x$  coordinate on the *cis* side for fixed values of  $D = 2$  and  $f = 100$  at different times  $t/\tau = 0.05 \dots 0.80$ . Panels (e) and (f) are the same as panel (d), but for other values of the channel width,  $D = 8$  and 64, respectively. To find  $v_x$  as a function of  $x$ , the *cis*-side channel is divided into parallel bins, and  $x$  denotes the location of the bins.  $x = 0$  indicates the location of the pore. The absolute value of  $x$  identifies the distance of the corresponding bin on the *cis* side from the pore.

In panel (g), the average velocity of monomer(s) inside the pore  $v_x(x = 0)$  is plotted as a function of the normalized time  $t/\tau$  for a fixed value of driving force  $f = 100$  and various values of  $D = 2 \dots 64$ . For each  $D$ , as time passes,  $v_x(x = 0)$  first decreases (in the TP stage where  $t < \tau_{TP}$ ), attains a minimum (transition from TP to the PP stage), and then increases (in the PP stage where  $t > \tau_{TP}$ ). As can be seen, in the TP stage and at a constant time, increasing  $D$  increases the velocity of monomers at the pore. In contrast, in the PP stage, as time passes, the velocity increases due to the reduction in the number of mobile monomers on the *cis* side. Moreover, in the PP stage, as time passes, the velocities eventually collapse onto a master curve. The results in panel (g) are in agreement with the waiting times presented in Fig. 2.

## REFERENCES

<sup>1</sup>S. M. Bezrukov, I. Vodyanoy, and V. Adrian Parsegian, "Counting polymers moving through a single ion channel," *Nature* **370**, 279 (1994).

- <sup>2</sup>J. Kasianowicz, E. Brandin, D. Branton, and D. W. Deamer, "Characterization of individual polynucleotide molecules using a membrane channel," *Proc. Natl. Acad. Sci. U. S. A.* **93**, 13770 (1996).
- <sup>3</sup>W. Sung and P. J. Park, "Polymer translocation through a pore in a membrane," *Phys. Rev. Lett.* **77**, 783 (1996).
- <sup>4</sup>M. Muthukumar, *Polymer Translocation* (Taylor & Francis, 2011).
- <sup>5</sup>V. V. Palyulin, T. Ala-Nissila, and R. Metzler, "Polymer translocation: The first two decades and the recent diversification," *Soft Matter* **10**, 9016 (2014).
- <sup>6</sup>J. Sarabadani and T. Ala-Nissila, "Theory of pore-driven and end-pulled polymer translocation dynamics through a nanopore: An overview," *J. Phys.: Condens. Matter* **30**, 274002 (2018).
- <sup>7</sup>A. Milchev, "Single-polymer dynamics under constraints: Scaling theory and computer experiment," *J. Phys.: Condens. Matter* **23**, 103101 (2011).
- <sup>8</sup>M. Muthukumar, "Polymer translocation through a hole," *J. Chem. Phys.* **111**, 10371 (1999).
- <sup>9</sup>J. Chuang, Y. Kantor, and M. Kardar, "Anomalous dynamics of translocation," *Phys. Rev. E* **65**, 011802 (2001).
- <sup>10</sup>F. Tessier and G. W. Slater, "Strategies for the separation of polyelectrolytes based on non-linear dynamics and entropic ratchets in a simple microfluidic device," *Appl. Phys. A* **75**, 285 (2002).
- <sup>11</sup>Y. Kantor and M. Kardar, "Anomalous dynamics of forced translocation," *Phys. Rev. E* **69**, 021806 (2004).
- <sup>12</sup>T. Ambjörnsson and R. Metzler, "Chaperone-assisted translocation," *Phys. Biol.* **1**, 77 (2004).
- <sup>13</sup>R. Zandi, D. Reguera, J. Rudnick, and W. M. Gelbart, "What drives the translocation of stiff chains?," *Proc. Natl. Acad. Sci. U. S. A.* **100**, 8649 (2003).
- <sup>14</sup>A. Y. Grosberg, S. Nechaev, M. Tamm, and O. Vasilyev, "How long does it take to pull an ideal polymer into a small hole?," *Phys. Rev. Lett.* **96**, 228105 (2006).

- <sup>15</sup>K. Luo, T. Ala-Nissila, and S.-C. Ying, "Polymer translocation through a nanopore: A two-dimensional Monte Carlo study," *J. Chem. Phys.* **124**, 034714 (2006).
- <sup>16</sup>T. Sakaue, "Nonequilibrium dynamics of polymer translocation and straightening," *Phys. Rev. E* **76**, 021803 (2007).
- <sup>17</sup>K. Luo, T. Ala-Nissila, S.-C. Ying, and A. Bhattacharya, "Influence of polymer-pore interactions on translocation," *Phys. Rev. Lett.* **99**, 148102 (2007).
- <sup>18</sup>G. Sigalov, J. Comer, G. Timp, and A. Aksimentiev, "Detection of DNA sequences using an alternating electric field in a nanopore capacitor," *Nano Lett.* **8**, 56 (2008).
- <sup>19</sup>M. G. Gauthier and G. W. Slater, "Nondriven polymer translocation through a nanopore: Computational evidence that the escape and relaxation processes are coupled," *Phys. Rev. E* **79**, 021802 (2009).
- <sup>20</sup>K. Luo, R. Metzler, T. Ala-Nissila, and S.-C. Ying, "Polymer translocation out of confined environments," *Phys. Rev. E* **80**, 021907 (2009).
- <sup>21</sup>K. Luo, T. Ala-Nissila, S.-C. Ying, and R. Metzler, "Driven polymer translocation through nanopores: Slow-vs.-fast dynamics," *Europhys. Lett.* **88**, 68006 (2009).
- <sup>22</sup>K. Luo and R. Metzler, "Polymer translocation into laterally unbounded confined environments," *J. Chem. Phys.* **133**, 075101 (2010).
- <sup>23</sup>K. Luo and R. Metzler, "Polymer translocation into a fluidic channel through a nanopore," *Phys. Rev. E* **82**, 021922 (2010).
- <sup>24</sup>T. Sakaue, "Sucking genes into pores: Insight into driven translocation," *Phys. Rev. E* **81**, 041808 (2010).
- <sup>25</sup>H. W. de Haan and G. W. Slater, "Mapping the variation of the translocation  $\alpha$  scaling exponent with nanopore width," *Phys. Rev. E* **81**, 051802 (2010).
- <sup>26</sup>P. Rowghanian and A. Y. Grosberg, "Force-driven polymer translocation through a nanopore: An old problem revisited," *J. Phys. Chem. B* **115**, 14127 (2011).
- <sup>27</sup>J. A. Cohen, A. Chaudhuri, and R. Golestanian, "Active polymer translocation through flickering pores," *Phys. Rev. Lett.* **107**, 238102 (2011).
- <sup>28</sup>K. Luo and R. Metzler, "The chain sucker: Translocation dynamics of a polymer chain into a long narrow channel driven by longitudinal flow," *J. Chem. Phys.* **134**, 135102 (2011).
- <sup>29</sup>T. Saito and T. Sakaue, "Process time distribution of driven polymer transport," *Phys. Rev. E* **85**, 061803 (2012).
- <sup>30</sup>T. Ikonen, A. Bhattacharya, T. Ala-Nissila, and W. Sung, "Unifying model of driven polymer translocation," *Phys. Rev. E* **85**, 051803 (2012).
- <sup>31</sup>T. Ikonen, A. Bhattacharya, T. Ala-Nissila, and W. Sung, "Influence of non-universal effects on dynamical scaling in driven polymer translocation," *J. Chem. Phys.* **137**, 085101 (2012).
- <sup>32</sup>H. W. de Haan and G. W. Slater, "Using an incremental mean first passage approach to explore the viscosity dependent dynamics of the unbiased translocation of a polymer through a nanopore," *J. Chem. Phys.* **136**, 204902 (2012).
- <sup>33</sup>H. Yong, Y. Wang, S. Yuan, B. Xu, and K. Luo, "Driven polymer translocation through a cylindrical nanochannel: Interplay between the channel length and the chain length," *Soft Matter* **8**, 2769 (2012).
- <sup>34</sup>N. Nikoofard, H. Khalilian, and H. Fazli, "Directed translocation of a flexible polymer through a cone-shaped nano-channel," *J. Chem. Phys.* **139**, 074901 (2013).
- <sup>35</sup>J. Sarabadani, T. Ikonen, and T. Ala-Nissila, "Iso-flux tension propagation theory of driven polymer translocation: The role of initial configurations," *J. Chem. Phys.* **141**, 214907 (2014).
- <sup>36</sup>A. Suma, A. Rosa, and C. Micheletti, "Pore translocation of knotted polymer chains: How friction depends on knot complexity," *ACS Macro Lett.* **4**, 1420 (2015).
- <sup>37</sup>R. Adhikari and A. Bhattacharya, "Translocation of a semiflexible polymer through a nanopore in the presence of attractive binding particles," *Phys. Rev. E* **92**, 032711 (2015).
- <sup>38</sup>J. Sarabadani, T. Ikonen, and T. Ala-Nissila, "Theory of polymer translocation through a flickering nanopore under an alternating driving force," *J. Chem. Phys.* **143**, 074905 (2015).
- <sup>39</sup>A. Fiasconaro, J. J. Mazo, and F. Falo, "Active polymer translocation in the three-dimensional domain," *Phys. Rev. E* **91**, 022113 (2015).
- <sup>40</sup>T. Menais, S. Mossa, and A. Buhot, "Polymer translocation through nano-pores in vibrating thin membranes," *Sci. Rep.* **6**, 38558 (2016).
- <sup>41</sup>J. Sarabadani, B. Ghosh, S. Chaudhury, and T. Ala-Nissila, "Dynamics of end-pulled polymer translocation through a nanopore," *Europhys. Lett.* **120**, 38004 (2017).
- <sup>42</sup>A. Suma and C. Micheletti, "Pore translocation of knotted DNA rings," *Proc. Natl. Acad. Sci. U. S. A.* **114**(15), E2991 (2017).
- <sup>43</sup>J. Sarabadani, T. Ikonen, H. Mökkönen, T. Ala-Nissila, S. Carson, and M. Wanunu, "Driven translocation of a semi-flexible polymer through a nanopore," *Sci. Rep.* **7**, 7423 (2017).
- <sup>44</sup>T. Menais, "Polymer translocation under a pulling force: Scaling arguments and threshold forces," *Phys. Rev. E* **97**, 022501 (2018).
- <sup>45</sup>S. Buyukdagli, J. Sarabadani, and T. Ala-Nissila, "Dielectric trapping of biopolymers translocating through insulating membranes," *Polymers* **10**, 1242 (2018).
- <sup>46</sup>S. Buyukdagli, J. Sarabadani, and T. Ala-Nissila, "Theoretical modeling of polymer translocation: From the electrohydrodynamics of short polymers to the fluctuating long polymers," *Polymers* **11**, 118 (2019).
- <sup>47</sup>A. Bhattacharya and S. Seth, "Tug of war in a double-nanopore system," *Phys. Rev. E* **101**, 052407 (2020).
- <sup>48</sup>J. Sarabadani, S. Buyukdagli, and T. Ala-Nissila, "Pulling a DNA molecule through a nanopore embedded in an anionic membrane: Tension propagation coupled to electrostatics," *J. Phys.: Condens. Matter* **32**, 385101 (2020).
- <sup>49</sup>B. Ghosh, J. Sarabadani, S. Chaudhury, and T. Ala-Nissila, "Pulling a folded polymer through a nanopore," *J. Phys.: Condens. Matter* **33**, 015101 (2020).
- <sup>50</sup>H. Khalilian, J. Sarabadani, and T. Ala-Nissila, "Polymer translocation through a nanopore assisted by an environment of active rods," *Phys. Rev. Res.* **3**, 013080 (2021).
- <sup>51</sup>J. Sarabadani, R. Metzler, and T. Ala-Nissila, "Driven polymer translocation into a channel: Isoflux tension propagation theory and Langevin dynamics simulations," *Phys. Rev. Res.* **4**, 033003 (2022).
- <sup>52</sup>A. Rezaie-Dereshgi, H. Khalilian, and J. Sarabadani, "Translocation of an active polymer into a two dimensional circular nano-container," *J. Phys.: Condens. Matter* **35**, 355101 (2023).
- <sup>53</sup>H. Khalilian, J. Sarabadani, and T. Ala-Nissila, "Polymer translocation in an environment of active rods," *Phys. Rev. Res.* **5**, 023107 (2023).
- <sup>54</sup>A. Meller, L. Nivon, and D. Branton, "Voltage-driven DNA translocations through a nanopore," *Phys. Rev. Lett.* **86**, 3435 (2001).
- <sup>55</sup>A. F. Sauer-Budge, J. A. Nyamwanda, D. K. Lubensky, and D. Branton, "Unzipping kinetics of double-stranded DNA in a nanopore," *Phys. Rev. Lett.* **90**, 238101 (2003).
- <sup>56</sup>A. J. Storm, J. H. Chen, X. S. Ling, H. W. Zandbergen, and C. Dekker, "Fabrication of solid-state nanopores with single-nanometre precision," *Nat. Mater.* **2**, 537 (2003).
- <sup>57</sup>M. Bates, M. Burns, and A. Meller, "Dynamics of DNA molecules in a membrane channel probed by active control techniques," *Biophys. J.* **84**, 2366 (2003).
- <sup>58</sup>U. F. Keyser, B. N. Koeleman, S. van Dorp, D. Krapf, R. M. M. Smeets, S. G. Lemay, N. H. Dekker, and C. Dekker, "Direct force measurements on DNA in a solid-state nanopore," *Nat. Phys.* **2**, 473 (2006).
- <sup>59</sup>E. H. Trepagnier, A. Radenovic, D. Sivak, P. Geissler, and J. Liphardt, "Controlling DNA capture and propagation through artificial nanopores," *Nano Lett.* **7**, 2824 (2007).
- <sup>60</sup>S. van Dorp, U. F. Keyser, N. H. Dekker, C. Dekker, and S. G. Lemay, "Origin of the electrophoretic force on DNA in solid-state nanopores," *Nat. Phys.* **5**, 347 (2009).
- <sup>61</sup>C. Raillon, P. Granjon, M. Graf, L. J. Steinbock, and A. Radenovic, "Fast and automatic processing of multi-level events in nanopore translocation experiments," *Nanoscale* **4**, 4916 (2012).
- <sup>62</sup>R. I. Stefureac, A. Kachayev, and J. S. Lee, "Modulation of the translocation of peptides through nanopores by the application of an AC electric field," *Chem. Commun.* **48**, 1928 (2012).
- <sup>63</sup>F. Traversi, C. Raillon, S. M. Benameur, K. Liu, S. Khlybov, M. Tosun, D. Krasnozhan, A. Kis, and A. Radenovic, "Detecting the translocation of DNA through a nanopore using graphene nanoribbons," *Nat. Nanotechnol.* **8**, 939 (2013).

- <sup>64</sup>R. D. Bulushev, S. Marion, and A. Radenovic, "Relevance of the drag force during controlled translocation of a DNA-protein complex through a glass nanocapillary," *Nano Lett.* **15**, 7118 (2015).
- <sup>65</sup>S. Nakielny and G. Dreyfuss, "Transport of proteins and RNAs in and out of the nucleus," *Cell* **99**, 677 (1999).
- <sup>66</sup>H. Ochman, J. G. Lawrence, and E. A. Groisman, "Lateral gene transfer and the nature of bacterial innovation," *Nature* **405**, 299 (2000).
- <sup>67</sup>L. Messenger, J. R. Burns, J. Kim, D. Cecchin, J. Hindley, A. L. B. Pyne, J. Gaitsch, G. Battaglia, and S. Howorka, "Biomimetic hybrid nanocontainers with selective permeability," *Angew. Chem., Int. Ed.* **55**, 11106 (2016).
- <sup>68</sup>D. Branton *et al.*, "The potential and challenges of nanopore sequencing," *Nat. Biotechnol.* **26**, 1146 (2008).
- <sup>69</sup>D. Deamer, M. Akeson, and D. Branton, "Three decades of nanopore sequencing," *Nat. Biotechnol.* **34**, 518 (2016).
- <sup>70</sup>F. Ritort, "Single-molecule experiments in biological physics: Methods and applications," *J. Phys.: Condens. Matter* **18**, R531 (2006).
- <sup>71</sup>R. D. Bulushev, L. J. Steinbock, S. Khlybov, J. F. Steinbock, U. F. Keyser, and A. Radenovic, "Measurement of the position-dependent electrophoretic force on DNA in a glass nanocapillary," *Nano Lett.* **14**, 6606 (2014).
- <sup>72</sup>R. D. Bulushev, S. Marion, E. Petrova, S. J. Davis, S. J. Maerkl, and A. Radenovic, "Single molecule localization and discrimination of DNA-protein complexes by controlled translocation through nanocapillaries," *Nano Lett.* **16**, 7882 (2016).
- <sup>73</sup>M. Muthukumar, "Translocation of a confined polymer through a hole," *Phys. Rev. Lett.* **86**, 3188 (2001).
- <sup>74</sup>A. Cacciuto and E. Luijten, "Self-avoiding flexible polymers under spherical confinement," *Nano Lett.* **6**, 901 (2006).
- <sup>75</sup>D. Sean, H. W. de Haan, and G. W. Slater, "Translocation of a polymer through a nanopore starting from a confining nanotube," *Electrophoresis* **36**, 682 (2015).
- <sup>76</sup>J. O. Tegenfeldt, C. Prinz, R. L. Huang, R. H. Austin, S. Y. Chou, E. C. Cox, J. C. Sturm, and H. Cao, "Micro- and nanofluidics for DNA analysis," *Anal. Bioanal. Chem.* **378**, 1678 (2004).
- <sup>77</sup>J. O. Tegenfeldt, C. Prinz, H. Cao, S. Chou, W. W. Reisner, R. Riehn, Y. M. Wang, E. C. Cox, J. C. Sturm, P. Silberzan, and R. H. Austin, "The dynamics of genomic-length DNA molecules in 100-nm channels," *Proc. Natl. Acad. Sci. U. S. A.* **101**, 10979 (2004).
- <sup>78</sup>Y. M. Wang, J. O. Tegenfeldt, W. Reisner, R. Riehn, X.-J. Guan, I. Golding, E. C. Cox, J. Sturm, and R. H. Austin, "Single-molecule studies of repressor-DNA interactions show long-range interactions," *Proc. Natl. Acad. Sci. U. S. A.* **102**, 9797 (2005).
- <sup>79</sup>R. H. Liu and A. P. Lee, *Integrated Biochips for DNA Analysis* (Springer 2007), Chap. 12.
- <sup>80</sup>F. Persson and J. O. Tegenfeldt, "DNA in nanochannels—Directly visualizing genomic information," *Chem. Soc. Rev.* **39**, 985 (2010).
- <sup>81</sup>S. Plimpton, "Fast parallel algorithms for short-range molecular dynamics," *J. Comput. Phys.* **117**, 1 (1995).
- <sup>82</sup>G. S. Grest and K. Kremer, "Molecular dynamics simulation for polymers in the presence of a heat bath," *Phys. Rev. A* **33**, 3628 (1986).
- <sup>83</sup>J. D. Weeks, D. Chandler, and H. C. Andersen, "Role of repulsive forces in determining the equilibrium structure of simple liquids," *J. Chem. Phys.* **54**, 5237 (1971).
- <sup>84</sup>J. Mathé, H. Visram, V. Viasnoff, Y. Rabin, and A. Meller, "Nanopore unzipping of individual DNA hairpin molecules," *Biophys. J.* **87**, 3205 (2004).
- <sup>85</sup>T. Ikonen, J. Shin, W. Sung, and T. Ala-Nissila, "Polymer translocation under time-dependent driving forces: Resonant activation induced by attractive polymer-pore interactions," *J. Chem. Phys.* **136**, 205104 (2012).
- <sup>86</sup>P.-G. de Gennes, *Scaling Concepts in Polymer Physics* (Cornell University Press, 1979).
- <sup>87</sup>J.-P. Bouchaud, "Weak ergodicity breaking and aging in disordered systems," *J. Phys. I* **2**, 1705 (1992).
- <sup>88</sup>E. Barkai, Y. Garini, and R. Metzler, "Strange kinetics of single molecules in living cells," *Phys. Today* **65**(8), 29 (2012).
- <sup>89</sup>R. Metzler, J.-H. Jeon, A. G. Cherstvy, and E. Barkai, "Anomalous diffusion models and their properties: Non-stationarity, non-ergodicity, and ageing at the centenary of single particle tracking," *Phys. Chem. Chem. Phys.* **16**, 24128 (2014).
- <sup>90</sup>Y. He, S. Burov, R. Metzler, and E. Barkai, "Random time-scale invariant diffusion and transport coefficients," *Phys. Rev. Lett.* **101**, 058101 (2008).
- <sup>91</sup>J.-H. Jeon and R. Metzler, "Inequivalence of time and ensemble averages in ergodic systems: Exponential versus power-law relaxation in confinement," *Phys. Rev. E* **85**, 021147 (2012).
- <sup>92</sup>A. Rosa, M. Di Ventra, and C. Micheletti, "Topological jamming of spontaneously knotted polyelectrolyte chains driven through a nanopore," *Phys. Rev. Lett.* **109**, 118301 (2012).
- <sup>93</sup>C. Micheletti and E. Orlandini, "Knotting and unknotting dynamics of DNA strands in nanochannels," *ACS Macro Lett.* **3**, 876 (2014).
- <sup>94</sup>Y. Wang, D. R. Tree, and K. D. Dorfman, "Simulation of DNA extension in nanochannels," *Macromolecules* **44**, 6594 (2011).
- <sup>95</sup>G. K. Cheong, X. Li, and K. D. Dorfman, "Evidence for the extended de Gennes regime of a semiflexible polymer in slit confinement," *Phys. Rev. E* **97**, 022502 (2018).
- <sup>96</sup>M. Rubinstein and R. H. Colby, *Polymer Physics* (Oxford University Press, 2003).